Supporting information

Scalable, eco-friendly, and ultrafast solar steam evaporator fabricated by evolutional 3D printing

Suyuan Zhou,[a] Shaolong Huang,[a] Yan Ming,[b] Yaojia Long,[a] Huawei Liang,[a] Shuangchen Ruan,[a] Yu-Jia Zeng *[a] and Hongzhi Cui*[c]

[a] College of Physics and Optoelectronic Engineering, Shenzhen University, Shenzhen 518060, P. R. China. E-mail: yjzeng@szu.edu.cn;

[b] Department of Materials Science and Engineering, Shenzhen Key Laboratory for Additive Manufacturing of High-performance Materials, Southern University of Science and Technology, Shenzhen 518055, P. R. China

[c] Key Laboratory for Resilient Infrastructures of Coastal Cities (MOE), College of Civil and Transportation Engineering, Shenzhen University, Shenzhen 518060, P. R. China. E-mail: h.z.cui@szu.edu.cn

Experimental Section

Fabrication of 3DP-ISSG

The Stereolithography Apparatus (SLA) is a high speed and high precision 3D printing technology. The complete parts were printed using an UV laser and a liquid UV-cured photosensitive polymer photosensitive resin. A 405-nm CO_2 laser with the spot diameter of about 0.12-0.20 mm was used as the laser beam, which was controlled to scan the resin liquid surface layer by layer. The high efficiency interfacial solar steam generation was constructed by 3D printing (SLA, Stereolithography) using the industrial-grade 3D-SLA molding printer Lite600HD (Liantai Technology Co., LTD, Shanghai, China), with the resolution of 1 mm.

The platform size of the marble substrates was about 600×600×400 mm with galvanometer scanning mode. The white photosensitive resin 9400 was used as the matrix materials.

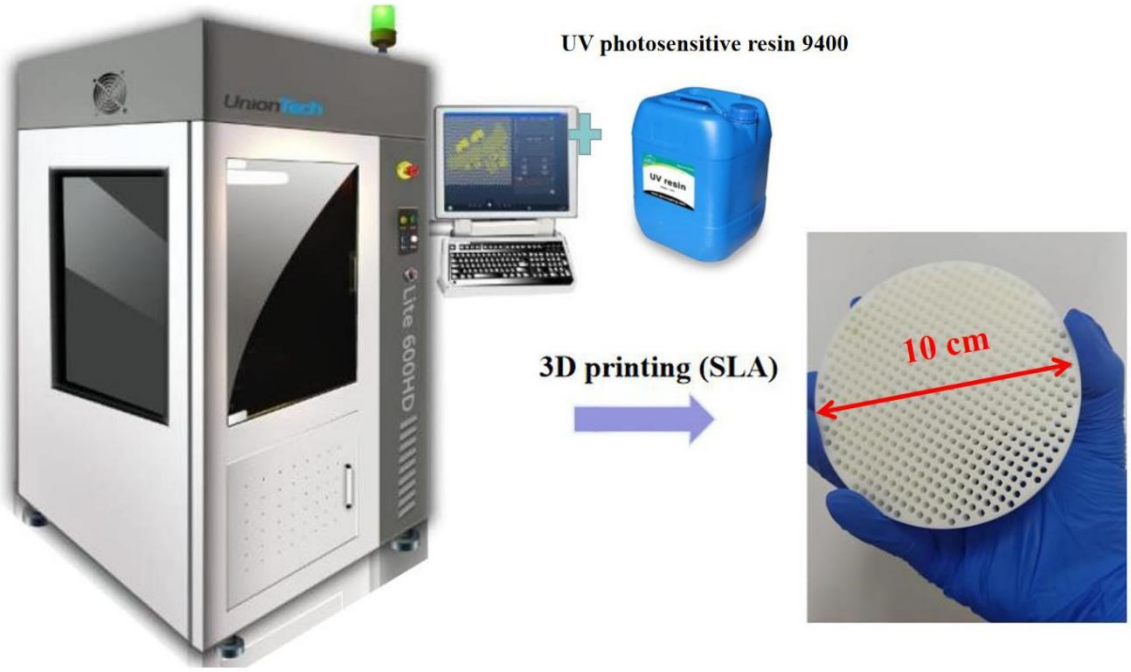

Figure S1. Industrial developed-3D SLA printer Lite600 HD with large specification (left) and Photograph of the large-scale 3D printing hexagonal interfacial solar steam generation (right).

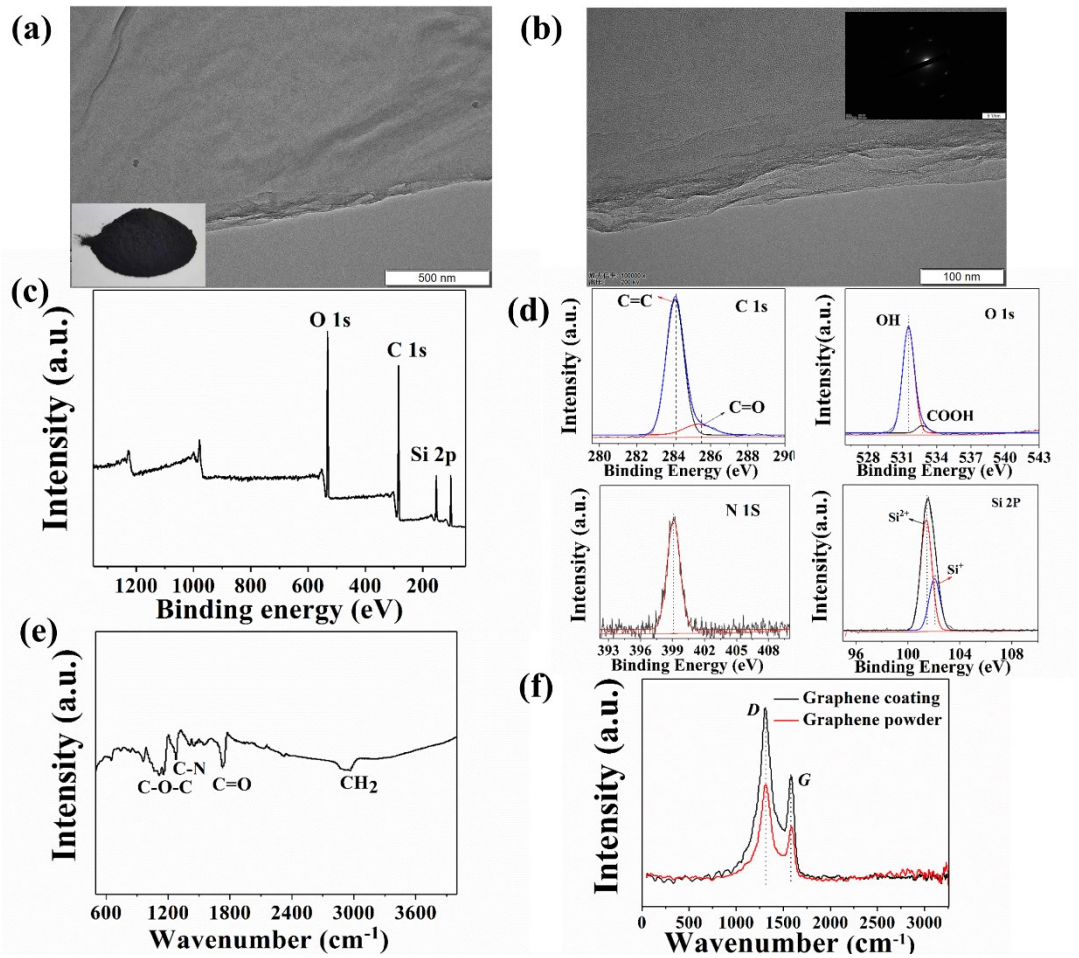

Figure.S2 Microstructure Characterization of graphene coating. (a)-(b) TEM images with different magnification, inset of (a): photograph of the as-prepared graphene powder; (c-d) XPS spectra of the graphene coating, (c) full spectra; (d) C 1s, O1s, N 1s and Si 2p, spectra. (e) FTIR spectrum of as-prepared graphene coating. (f) Raman spectrum for pristine graphene and the resulting graphene coating.

The commercial graphene was deposited on air-laid paper as PCM. In can be found that the agglomerated graphene has large-sized and compact multilayered structure with smooth surface and large packing densities, which can localize and absorb most part of solar-thermal energy due to the mirror reflection. Figure S2 (a) and (b) show TEM images of graphene with different magnifications. X-ray photoelectron spectroscopy (XPS) survey spectra were measured to examine the chemical compositions of the graphene coating after surface hydrophobic treatment as shown in Fig.S2 (c) The results reveal the presence of C1s, O 1s, Si

2p and N 1s in the coating. The C 1s peaks are located at 284.3 eV and 285.4 eV, which are close to standard value of graphene and C = O, respectively. The O1s peaks indicate two components centered at 531.4 and 532.6 eV, which are identified to the typical oxygen functional groups of CO and COOH, respectively. The Si 2p curve can be fitted into two peaks centered at 101.2 eV and 102.0 eV, corresponding to Si-O and Si-Ox groups, respectively. The N 1s peak is located at 399.4 eV, which corresponds to standard value of the pyrrolic (C–N–C).[1] FTIR spectrum of the graphene coating are shown in Fig. S2 (e). Four absorption characteristic peaks of symmetric and antisymmetric stretching vibrations are observed, i.e. CH_2 (2930 cm^{-1}), C=O (1725 cm^{-1}) stretching vibration peak on the carboxyl group and alkoxy epoxy C-N (1250 cm^{-1}) and vibration absorption peak of C-O (1110 cm^{-1}). These superficial C, O-related functional groups on the assembled graphene coating result from the surface hydrophobic treatment, which are beneficial to form various surface energy traps and generate additional band energies.[2] Fig. S2 (f) shows the Raman spectra of the graphene coating and graphene powder. Two strong characteristic peaks are observed corresponding to the D band (1351 cm^{-1}, defective carbon) and G band (1580 cm^{-1}, graphitic six-membered ring structure carbon).[3] The peak ratios of I_D/I_G are 1.83 and 1.7 for the graphene coating and graphene powder, respectively. This result indicates the overall deterioration of crystalline quality of the graphene coating.

Preparation of hydrophobic coatings

The hydrophobic coatings were fabricated with nano-SiO_2 and water-based acrylic acid resin GC-121 *via* a sol-gel process. Briefly, 2 g of as-synthesized curing agent amino epoxy resin GC-122 was added to 20 mL of distilled water. Then 1 g of nano SiO_2 ((15nm), purity 99.5%) purchased from Sigma-Aldrich (Shanghai, china) was slowly poured into the mixture solution sonicated for 0.5 h and stirred with a magnetic stirrer for 20 min. 2.02 g of water-based

acrylic acid resin GC-121 was added to the nano-SiO_2 / curing agent homogeneous solution. Then, the hydrophobic coating was prepared by stirring it with a magnetic stirrer for 30 min. A free-standing supernatant hydrophobic coating was obtained by spraying through the solution with subsequent drying in air.

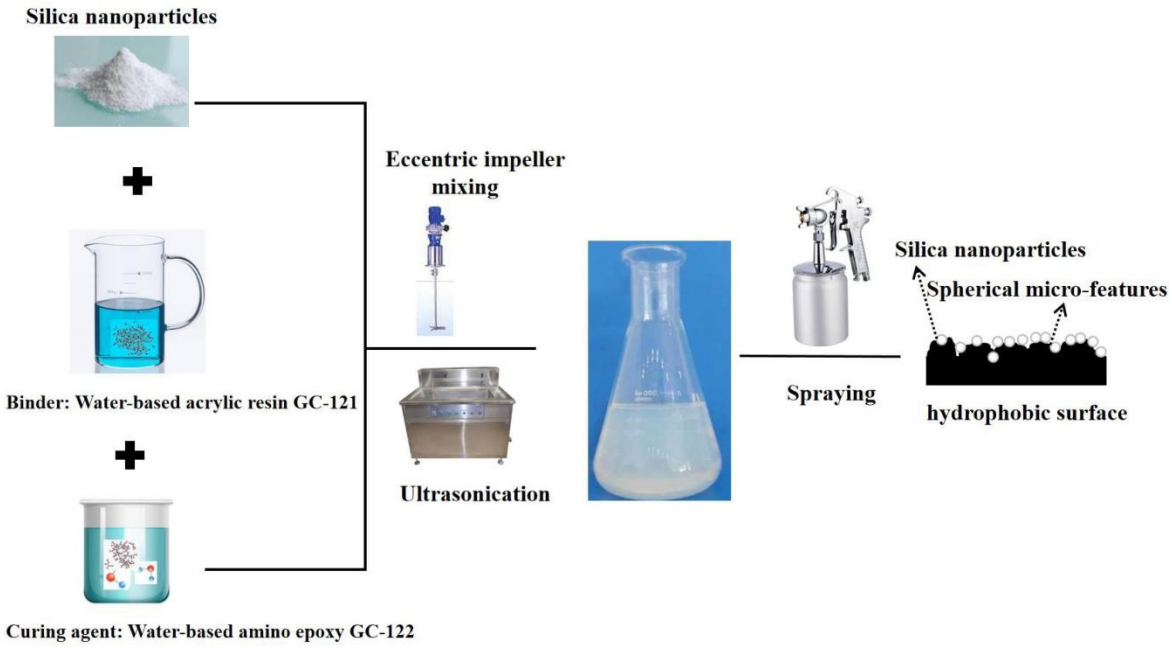

Figure.S3 Schematic illustration of experimental setup for hydrophobic ink synthesis.

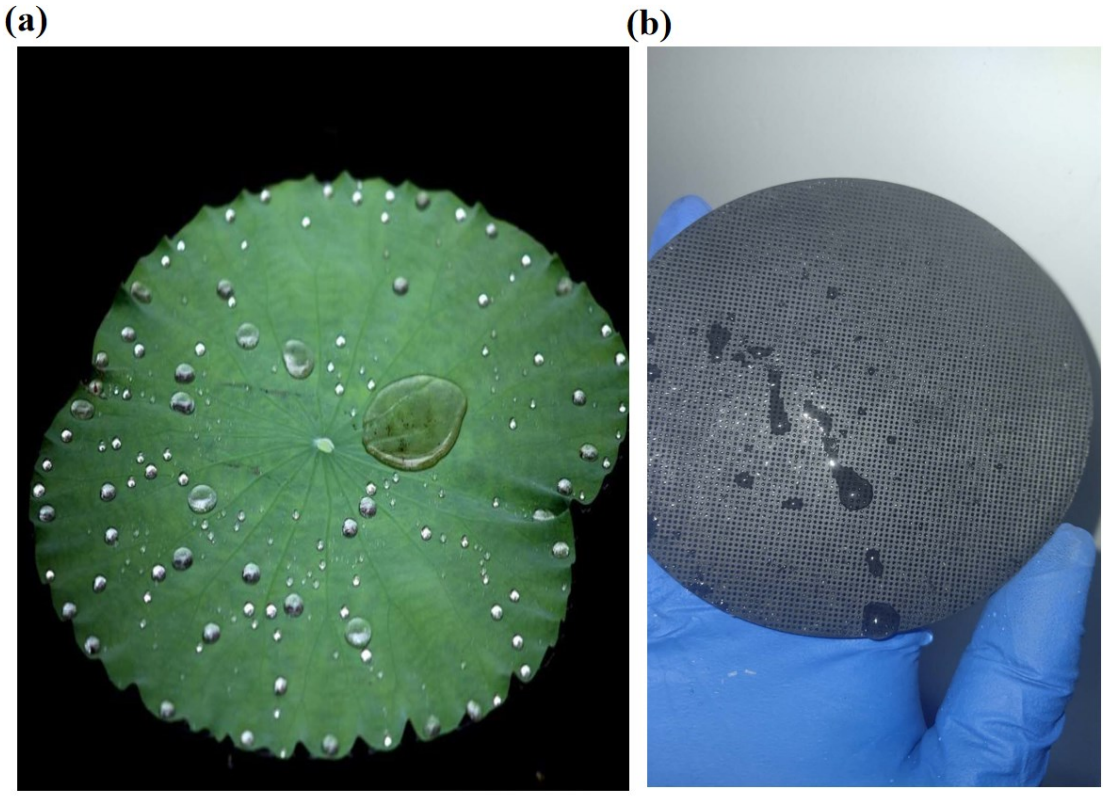

Figure S4. Hydrophobicity comparison between lotus leaf and solar evaporator surface of G@3DP-ISSGS

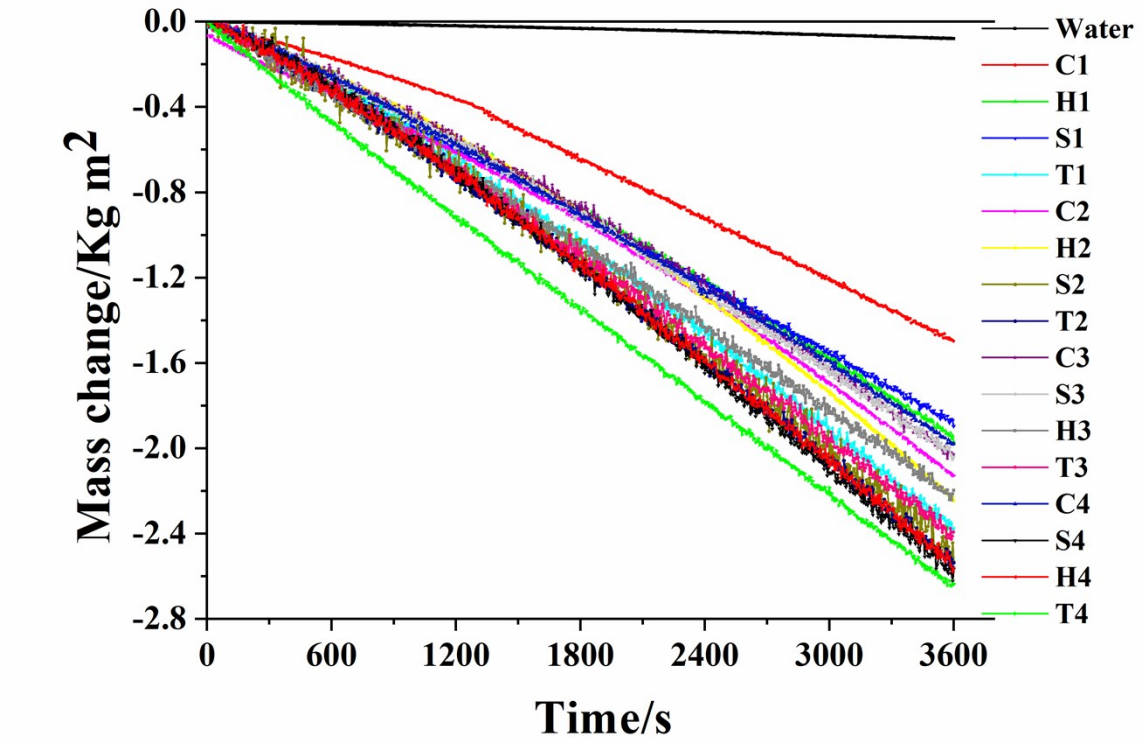

Figure S5. The mass loss of water for G@3DP-ISSGS devices with different cross section shapes and sizes of capillary in 1 hour under one sun (100 mW/cm^2). The pure water without devices is used as the control test

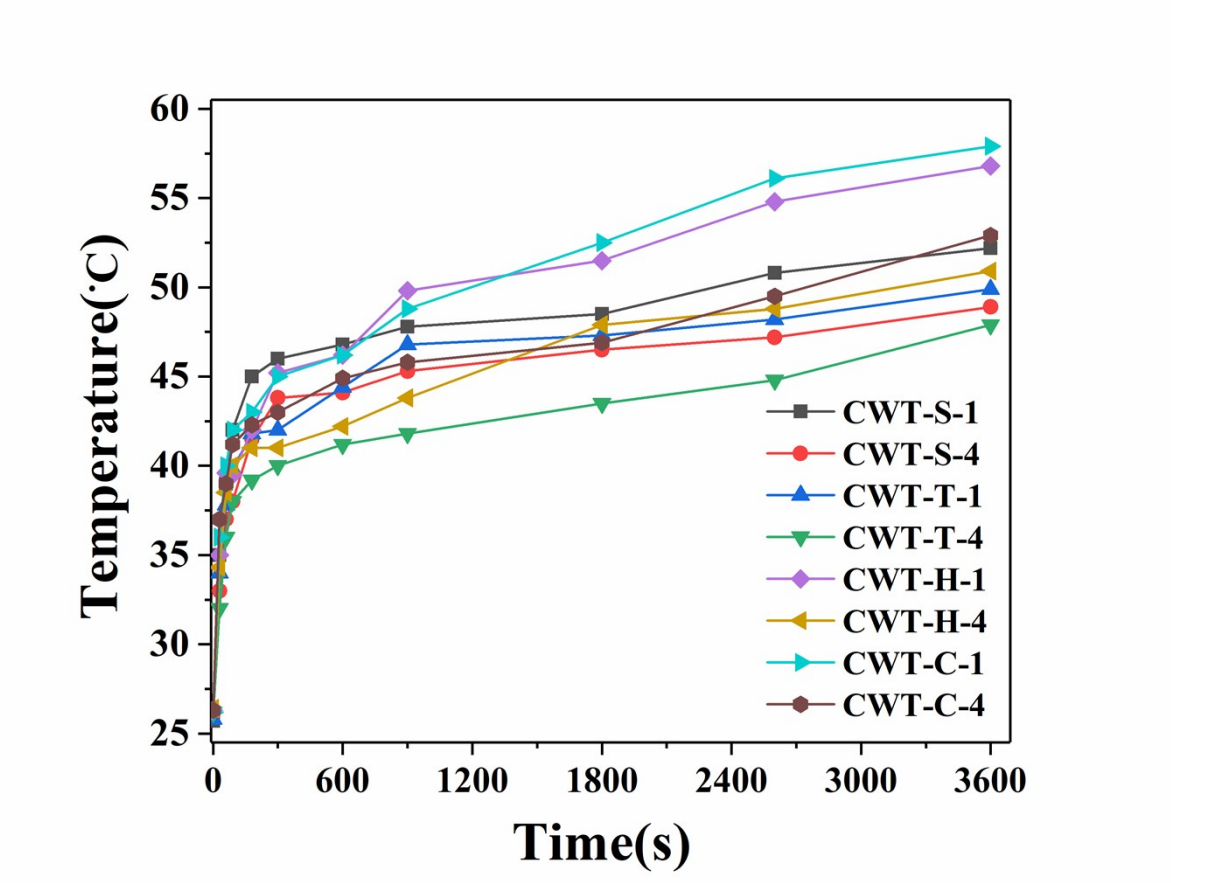

Figure S6. The surface temperatures of G@3DP-ISSGS devices with different shapes and sizes of capillary as a function of time under one solar radiation (100 mW/cm^2)

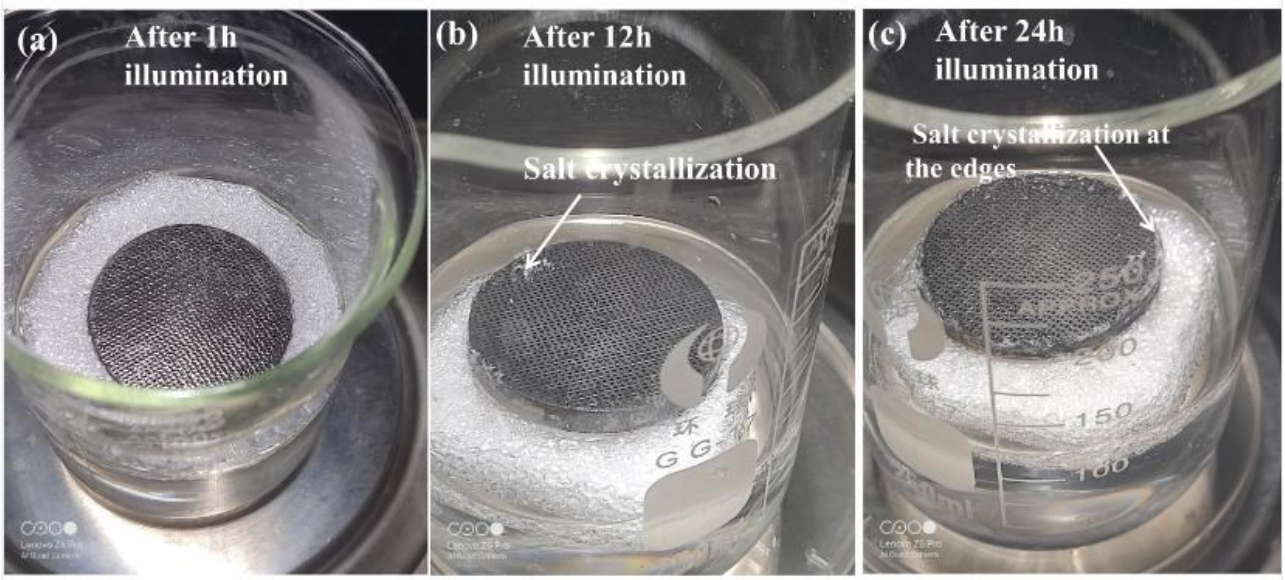

Figure S7. The process of anti-fouling property test. After 24h solar illumination (1 sun), no obvious contaminants were precipitated on the surface of G@3DP-ISSGS-T-4.

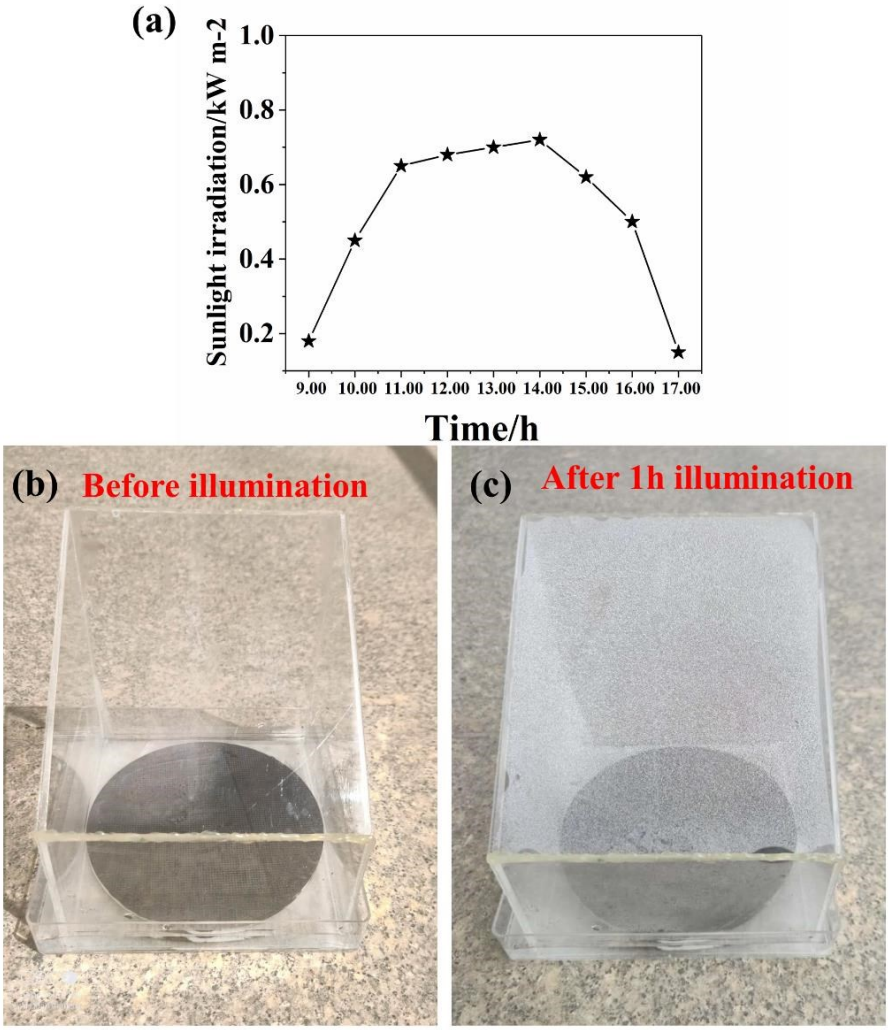

Figure S8. (a) The outdoor experiment of the vapor generation device in the natural sunlight from 9:00 to 10:00 o'clock with an average heat flux of 0.52 kW m^{-2} (16 October 2020). (b) The G@3DP-ISSGS-C floats on the seawater in a container. The vapor is condensed via the transparent condenser and flows to the bottom of the holder, where the purified water is stored. (c) After 1 h, the water droplets are covered over the whole condenser walls.

Calculation S1. The equivalent vaporization enthalpy of G@3DP-ISSGS

The latent heat λ_{lv} is dependent on the temperature (T_i) of the water/air interface where the vaporization occurs.[4,5] which is calculated by an empirical formula (1).[6,7] The latent heat of G@3DP-ISSGS devices with different shapes and sizes of capillary as a function of surface temperatures under one solar radiation for the empirical calculation are shown in Figure S6

$$\lambda_{lv} = 1.91846 \times 10^6 \left\{ T_i / (T_i - 33.91) \right\}^2 \quad (1)$$

the T_i is the temperature of the water/air interface (K). The sensible heat of water is calculated by the equation: $Q = C_p (T_i - T_s)$, where C_p is the specific heat capacityof water (4.2 kJ kg^{-1} K^{-1}), T_s is the temperature of the source water, which is 25.6°C (298.75 K) in our case.

Table S1. The surface temperature of G@3DP-ISSGS devices from Figure S6 with different shapes and sizes of capillary as a function oflatent heat specific heat, latent heat plus sensible heat, and the energy efficiency under one solar radiation for the calculation. The theoretical water evaporation rate is estimated by setting the energy efficiency to 100%.

	G@3DP-ISSGS-S-1	G@3DP-ISSGS-S-4	G@3DP-ISSGS-T-1	G@3DP-ISSGS-T-4	G@3DP-ISSGS-H-1	G@3DP-ISSGS-H-4	G@3DP-ISSGS-C-1	G@3DP-ISSGS-C-4
Latent heat (kJ kg^{-1})	2390.1	2396.6	2394.5	2398.3	2383.3	2393.1	2381.1	2389.7
sensible heat(kJ kg^{-1})	111.72	97.86	102.06	93.66	131.04	106.26	135.66	114.7
latent heat plus sensible heat (kJ kg^{-1})	2501.82	2494.46	2496.56	2491.96	2514.34	2499.36	2516.76	2504.4

energy conversion efficiency η	123.7%	172.53%	133.14%	178.5%	113.8%	161.7%	95.7%	139.8%

Calculation S2. Simulation of evaporative heat transfer under capillary action of different cross sections

The simulation of interfacial solar steam generation involves heat transfer and vapor transport in modeling the evaporation of the interface. The cross sections of the capillary tubes during evaporative heat transfer are equilateral, quadrilateral, hexagonal and circular, since the liquid-gas interfacial tension in the capillary will be attached to the liquid column according to the Laplace equation:

$$p = \frac{2\sigma}{\rho_1} \tag{2}$$

where P is the additional pressure (Pa), σ is the interface tension of liquid and gas (N/m), ρ_l indicates the axial curvature half diameters (m) of a meniscus curvature surface. When a capillary is in a liquid, the liquid would tend to wet the wall, thereby forming a "curved surface" in the capillary; Due to the $p = \frac{\gamma}{\cos\theta}$, γ denotes the equivalent radius (m) of the capillary tube, and θ denotes the solid-liquid contact angle, the additional pressure P applied to the capillary channel should be larger than or equal to the heavy force and thus can rise the liquid water in the capillary, where the analytical expression of H_{lf} is the height of the liquid front defined by the Lucas-Washburn equation：

$$H = \sqrt{\frac{\sigma\gamma_1 \cos\theta}{2\mu_w}} \tag{3}$$

where σ is the interface tension of liquid and gas (N/m), γ_1 denotes the equivalent radius (m), θ is the contact angle and μ_w is the dynamic viscosity of water. From the calculation of

equivalent radius to assess the capillary effect in the Fig, the capillary tubes formed by the cross-sectional of the triangle and quadrangle are the smallest and most likely to produce the capillary effect. The cross-sectional of the hexagon and circle are the least likely to produce capillary effect. In the same dimension of the section, the shapes of each parts of the aligned capillary water pathways were changed, and the capillary equivalent diameters were also changed. When the size of cross-sectional of 3DP-ISSGS decreases, the capillary tube is increased in equivalent diameter, which is beneficial to the transmission of liquid water.

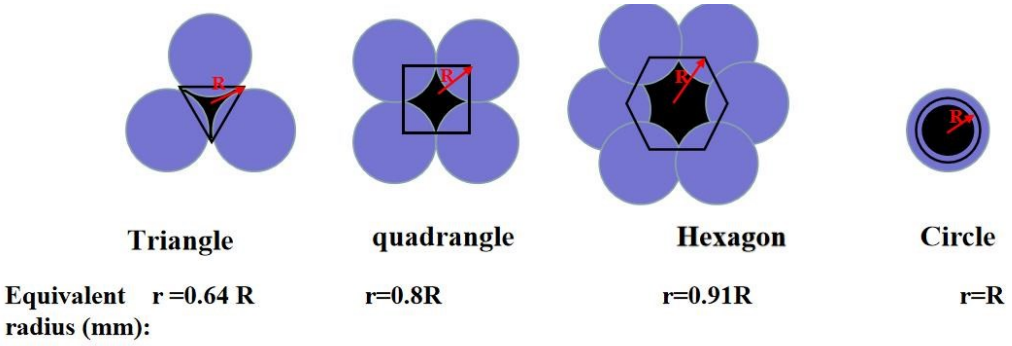

The model calculated the equivalent radius of capillary tubes under different cross section shapes.

Calculation S3. COMSOL Simulation of water transport in 3DP-ISSG

Numerical simulations were conducted by COMSOL Multiphysics 5.5 under the transient analysis mode. The essence of the model we established was that the fluid flows in the porous medium. We considered the porosity of the porous 3DP-ISSG as equal and ignored the complexity caused by deformation and channel bending to derive the transient state model of fluid transport. The capillary forces dominate over gravity throughout the simulation, the deformation of the water surface induces surface tension at the air/water

interface, which in turn creates a pressure jump across the interface. The pressure variations cause the water and air to move upward. The fluids continue to rise until the capillary forces are balanced by the gravity force.

The model consists of a capillary channel of radius 0.5 mm attached to a water reservoir and is based on the equations for the convection of the interface. The level set function can thus be considered as the volume fraction of water. The two-phase flow dynamics is governed by a Cahn-Hilliard equation. The equation tracks a diffuse interface separating the immiscible phases. [3,4]

$$\frac{\partial \phi}{\partial t} + u \cdot \nabla \phi = \nabla \cdot \frac{\gamma \lambda}{\varepsilon^2} \nabla \left(-\nabla \cdot \varepsilon^2 \nabla \phi + \phi(\phi^2 - 1) \right) \tag{4}$$

The parameter ε was typically used as an interface thickness of characteristic of mesh size in the region. where **u** is the fluid velocity (m/s), γ is the mobility ($m^3 \cdot s/kg$).

The diffuse interface is defined as the region where the dimensionless phase field variable ϕ goes from 0 to 1. Although the critical two-phase flow adiabatic capillary tube is nonlinear under some conditions, its mass flow characteristics show good linearity. The conservation of momentum of the water fluid in the internal microporous porous channel network in the 3DP-ISSG are depicted by the Navier-Stokes equations as follow: [8,9]

$$\rho \frac{\partial u}{\partial t} + \rho(u \cdot \nabla)u = \nabla \cdot \left[-pI + \mu(\nabla u + (\nabla u)^T) \right] + F_{st} + \rho g \tag{5}$$

$$\nabla \cdot u = 0 \tag{6}$$

where ρ is the fluid density; **u** and t stand for the fluid flow speed of water phase and time, respectively; and **g** is the gravity vector (m/s^2), P represents the intrinsic fluid pressure, comprising the osmotic pressure and the remaining part of the intrinsic entry capillary

pressure 1.6432e^5 N/m². F_{st} is the surface tension force acting at the air/water interface. The surface tension force is computed as: [10]

$$F_{st} = \sigma\delta\kappa n \tag{7}$$

Here, **n** is the interface normal, ***k*** is the curvature, σ is the surface tension coefficient (N/m), equals to a Dirac delta function that is nonzero only at the fluid interface.

where μ is the viscosity of the water at room temperature (293K, 1×10^{-3}Pa·s). The 3DP-ISSG structure with different shapes of capillary channel (triangle, quadrilateral, hexagon, circle) can be approximately regarded as circle using the same equivalent radius (mm). So, the 2D model can be discretized into a single unit for analysis. In laminar flow setting, surface boundary conditions were given on the flow rate of 1.47 kg m^{-2} h $^{-1}$/1000 kg m^{-3}), the bottom was set as free flow conditions. The solid surface was considered to be with no slip wall, so the velocity of water near solid was nearly zero. As a result, the simulation results showed that the center of the 3DP-ISSG-T-4 microchannel has the highest velocity 0.8 m/s.

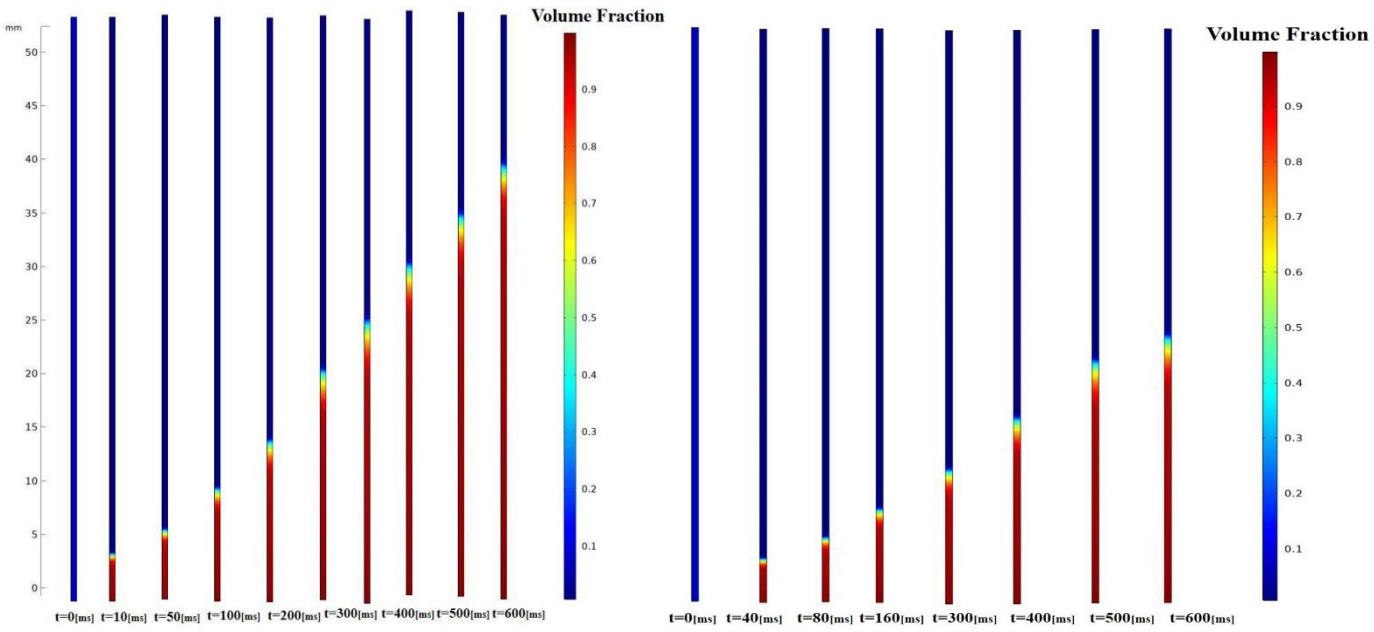

Water saturation in the capillary channel with the circle shape (left) and triangle shape (right) with the radius of about 0.4 mm.

COMSOL simulation of temperature distribution in 3DP-ISSG

Considering the water confinement of 3DP-ISSG and the convection in the micron channels, the heat transfer in 3DP-ISSG can be described by the equation: [7,8]

$$\rho_{eff}(C_{\rho}+C_{l})\frac{\partial T}{\partial t}=\nabla\cdot(\lambda_{ef}\nabla T)+Q-L_{V}g_{evap} \quad (8)$$

$$g_{evap}=k_{evp}M_{v} \quad (9)$$

The equations of the Heat Transfer in Solids interface with water transport in the 3DP-ISSG was solved for the transient temperature and evaporation rate, *T*, where ρ_{eff} is the density (SI unit: kg/m^3), *Cp* is the heat capacity (SI unit: J/(kg*K)), λ_{eff} is the thermal conductivity (SI unit: W/(m*K)), and *Q* represents the thermal energy input from the optical-thermal conversion (SI unit: W). K_{evp} is the evaporation rate and the molar mass of water vapor M_v are used. L_v is the latent heat of vaporization (SI unit: J/kg), x and t are the space vector and time, respectively; Heat energy is required for evaporation to occur, which is characterized in a heat source domain condition, ν and k stand for the fluid flow speed and thermal conductivity of the aqueous medium; ρ, C_l, and T (x, t) are the mass density, liquid thermal capacity and the local temperature, respectively; [9,10]

This COMSOL Multiphysics example couple evaporation interfaces describing the time-dependent temperature and the constant moisture concentration, respectively. The simulation does not model the convective velocity field outside the area because the coefficients for convective heat and moisture transfer to the surrounding air are given. The 3DP-ISSG diffusive processes of evaporation describe both heat transfer and moisture transport.[11,12] Considering the water confinement and the convection in the internal micron channels of epoxy resin, the model assumes that the specific heat capacity of water increases with temperature according to the expression:

$$C_{p}=1550+2.05\Delta T+0.24(\Delta T)^{2}+0.0024(\Delta T)^{3}(J/(kg\cdot K)) \quad (10)$$

The heat transfer model can be simplified as a semi-infinite medium for the Cartesian coordinate system.[12,13,14] The numerical simulations were conducted by COMSOL Multiphysics, modeling with Laminar Flow and Heat Transfer modules by finite element simulation software. [15,16,17] Wherein, a steady and constant heat flux of 100 mW cm^{-2} occurs on the top (Z = 500), corresponding to the solar energy input on the surface of 3DP-ISSG. The material structure can be approximately regarded as two-dimensional model that can be discretized into a single unit for analysis. The convection heat transfer of water microporous channels in the 3DP-ISSG could described by the flow of internal capillary and separate heat restriction effect. To carry out a qualitative analysis, we assumed that the temperature of environment and water as 20 ºC (293.15 K). In the heat transfer setting, the velocity calculated by the laminar flow interface was used as the convection velocity of heat transfer. Solid wall was set as the heat source conditions, the total thermal power equal to 100 mW cm^{-2}. The bottom temperature was set to 293.15 K. The parameters of common material water were used to calculate the material properties of fluid, and the thermal conductivity of solid is 0.03206 W m^{-1} K^{-1}. The simulation results showed that due to the continuous photothermal conversion (heating) and evaporation process (cooling) on the surface, the 3DP-ISSG surface temperature finally reached a dynamic stability, which was close to the experimental temperature.

Table. Material properties of 3DP-ISSG and water in liquid and vapor phases.[4,5]

Material	**Density (kg/m3)**	**Specific Heat Capacity (J/kg·k)**	**Thermal conductivity (W/m·k)**	**Viscosity (kg/m·s)**

Water (liquid)	1000	4182	0.6	0.0009
Water (vapor)	0.6	2014	0.026	1.34×10^{-5}
UV Photosensitive Resin 9400	1200	1470	0.19	

Table S2. Estimation of the total cost of the prototype with 1 m^2 G@3DP-ISSGS

The prices of all materials and the amount required for the prototype with 1 m^2 G@3DP-ISSGS are summarized in the table below:

Material	**Price ￥($)**	**Amount**	**Cost ($)**
3D printing Photosensitive resin	400 (**￥/kg**) 57.4 (**￥/kg**)	0.4kg	23
GNP ink	600(**￥/kg**) 86.1(**￥/kg**)	0.05kg	4.3

The total cost of the prototype with 1 m^2 G@3DP-ISSGS can be estimated to be: 23+4.3 = 27.3 dollars (https://www.1688.com/). As the technology of 3D printing advances, the corresponding cost will be further reduced.

References

1 M. S. Zielinski, J.-W. Choi, T. La Grange, M. Modestino, S. M. H. Hashemi, Y. Pu, S. Birkhold, J. A. Hubbell and D. Psaltis, Nano Lett., 2016, 16, 2159.

2 H. J. Cho, D. J. Preston, Y. Zhu, E. N. Wang, Nat. Rev. Mater. 2016, 2, 16092.

3 F. Zhao, X. Y. Zhou, Y. Shi, X. Qian, M. Alexander, X. P. Zhao, S. Mendez, R. Yang, L.T. Qu, G. Yu, Nat. Nanotechnol., 2018, 13, 489.

4 L. L. Zhu, M. M. Gao, C. K. N. Peh, G. W. Ho, Nano Energy, 2019, 57, 507.

5 X. Wu, T. Gao, C. H. Han, J. S. Xu, G. Owens, H. L. Xu, Sci. Bull., 2019, 64, 1625.

6 Henderson-Sellers, B. Q. J. R. Meteorol. Soc. 1984,110, 1186.

7 X. Q. Li, W. C. Xu, M. Y. Tang, L. Zhou, B. Zhu, S. Zhu, J. Zhu, P NATL ACAD SCI USA., 2016, 113, 13953.

8 Taheri M H, Goshayeshi H R. Asme International Mechanical Engineering Congress & Exposition. 2012.

9 Bahraseman H G, Languri E M, Proceeding of the ASME 2016 Power Conference, 2016, V001T08A008.

10 Laurindo, J.B, Bray, Y. Le, and Prat, M. American Society of Mechanical Engineers Heat Transfer Division Htd 1995.

11 Laurindo J B, Prat M. Chem. Eng. Sci., 1998, 53, 2257.

12 Laurindo J B, Prat M. Chem. Eng. Sci., 1996, 51, 5171.

13 Y.J. Yuan. Y.D. Yuan, Y.Y. Xu, Adv. Mater. Res 2012, 557, 2159.

14 I. Tanasawa, Advances in Heat Transfer 1991, 21, 55.

15 M.S. Anghelescu, Thermal and mechanical analysis of carbon foam, Ph.D. thesis, Ohio University, Athens, Ohio2009.

16 J.W.N. A.J. Duguay, A. Kiziltas, D.J. Gardner and H.J. Dagher, Appl Nanosci,2014, 4, 279.

17 Grinchik N N, Akulich P V, Adamovich A L, J Eng Thermophys, 2007, 80, 1.